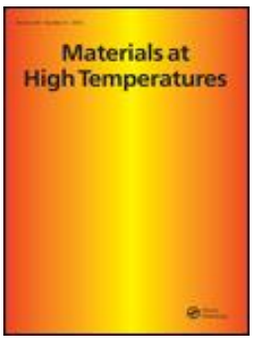

Materials at High Temperatures

ISSN: 0960-3409 (Print) 1878-6413 (Online) Journal homepage: http://www.tandfonline.com/loi/ymht20

Comparison between oxidation of Fe–Cr–Al sputter coatings in air and air–HCl environments at 550°C

D. Orlicka, N. J. Simms, T. Hussain & J. R. Nicholls

To cite this article: D. Orlicka, N. J. Simms, T. Hussain & J. R. Nicholls (2015) Comparison between oxidation of Fe–Cr–Al sputter coatings in air and air–HCl environments at 550°C, Materials at High Temperatures, 32:1-2, 167-176, DOI: 10.1179/0960340914Z.00000000095

To link to this article: http://dx.doi.org/10.1179/0960340914Z.00000000095

Published online: 19 Jan 2015.

Comparison between oxidation of Fe–Cr–Al sputter coatings in air and air–HCl environments at 550°C

D. Orlicka[1], N. J. Simms*[1], T. Hussain[2] and J. R. Nicholls[1]

In biomass fired power plants the superheaters and reheaters are known to be particularly susceptible to chloride induced fireside corrosion. One approach to giving them longer lives is to develop new coatings that are resistant to this type of fireside corrosion damage. This paper reports the initial stages of such an approach using the combinatorial model alloy development method. Physical vapour deposition (PVD) using a two-target magnetron sputtering system (99·95 wt-%Cr and Fe–30 wt-%Al) has been used to obtain a range of coating compositions. The coatings were deposited onto an array of sapphire discs (10 mm diameter; 3 mm thick) placed in front of the targets. This resulted in a group of samples with coatings with a range of different Cr to Fe/Al ratios, which have been characterised using scanning electron microscopy/energy dispersive X-ray analysis (SEM/EDX) and X-ray diffraction (XRD). Two groups of eleven coatings have been exposed at 550°C for up to 150 h in air and air–315 vppm HCl. Weight change data was gathered from these exposures after 50 and 150 h. After each exposure period, the surfaces of the oxidation/corrosion products were characterised using SEM/EDX and XRD. This analytical data has been used to identify the phases formed and the morphology of the scales generated. The best performing coatings from the mass change data were cross-sectioned to characterise the damage.

Keywords: High temperature oxidation, Fe–Cr–Al coatings, Oxidation in air, Oxidation in air with HCl, Biomass combustion

This article is part of a special issue on Microscopy of Oxidation 9

Introduction

Fossil fuels such as coal are still being used in large power plants as a major source of electricity. As a result of coal combustion significant amounts of CO_2 are produced and emitted to the atmosphere. CO_2 is known to be the main contributor to the greenhouse effect and global warming.[1] Therefore, renewable energy sources (RES), which are considered to be 'carbon-neutral', are of increasing interest for the EU to replace conventional fuels. In the last few years replacement of fossil fuels with biomass or waste has become a very attractive alternative because they are classified as having no net CO_2 contribution to the atmosphere.[1–4]

Biomass-fired power plants are designed to operate at lower steam temperatures and pressures than coal-fired plants to reduce the high corrosive damage rates found on their superheaters/reheaters. Hence, the efficiency of such plants is also expected to be much lower. Unfortunately, it is also true that higher fireside corrosion rates exist in plants co-firing high levels of biomass with coal, than in conventional fossil fuel power plants.[1,2,4,5] The biomass combustion environment is rich in gaseous HCl, alkali metals, calcium, oxygen, CO_2 and water vapour, but the SO_x content is typically low. Thus, corrosion is expected to occur through mechanisms which are different than those found in traditional coal-fired plants (e.g., alkali chloride and chromate formation instead of alkali iron tri-sulphate formation).[6,7] Gases containing chlorine in the form of HCl, Cl_2, NaCl or KCl can accelerate the fireside corrosion rate causing increased oxidation processes, metal wastage and/or defects in the metal structure.[8,9] The alkali chlorides have been reported to destroy protective chromium oxide scales by the formation of Na_2CrO_4 and K_2CrO_4, which cause depletion of chromium in the oxide scale leading to its breakdown.[10] The 'chlorine cycle' is frequently used to describe the role of chlorine in the corrosion environment.[11] Chlorides can also deposit on the tubes and influence the corrosion caused by the molten alkali sulphates or sulphidation typical of conventional coal fired plant fireside corrosion.[8]

As indicated above, alloys exposed to an aggressive environment are usually expected to form protective oxide layers, such as Cr_2O_3, which are able to resist any detrimental corrosion influence on the metal. The scale is protective when it has a continuous structure with

[1]Cranfield University, Cranfield, Bedfordshire, MK43 0AL, UK
[2]Faculty of Engineering, University of Nottingham, Nottingham, NG7 2RD, UK

*Corresponding author, email n.j.simms@cranfield.ac.uk

Received 16 April 2014; accepted 15 July 2014
DOI 10.1179/0960340914Z.00000000095

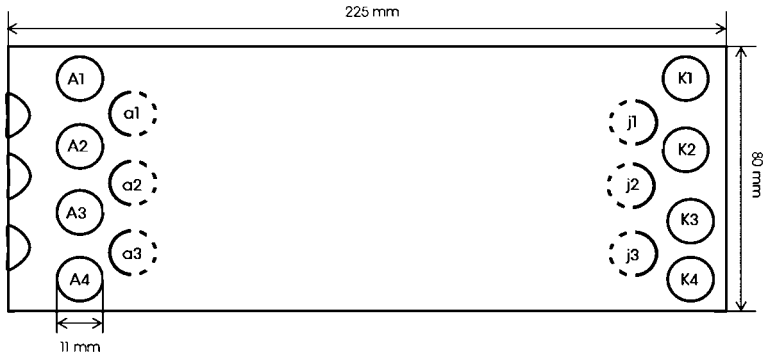

1 Sample holder used for two target co-sputtering trials showing sample locations:[21] samples used in these exposures were from rows A2-K2 and A4-K4

small concentration of defects, is adherent and characterised by a low growth rate.[12,13] The most popular materials used for the heat exchanger applications are ferritic (Fe–Cr) and austenitic (Fe–Cr–Ni) steels.[7] The oxides formed on low alloyed steels do not enable them to resist fireside corrosion even if HCl is not present.[14] In contrast, austenitic steels can form protective chromium oxide layers (Cr_2O_3).[7] The fireside corrosion resistance of these materials can be improved by the addition of other alloying elements, such as Al or Si[11] which can enable the formation of thermodynamically stable oxides (Al_2O_3, SiO_2).[15] It has been found that Fe–Cr–Al alloys have very good oxidation and corrosion resistance at elevated temperatures because of their tendency to form protective α-alumina layer (which are known to inhibit the oxidation and corrosion processes).[13,15–17] Extensive experiments into Fe–Cr–Al behaviour have included evaluating the levels of chromium and aluminium required to allow Al_2O_3 scale formation. Specifically, the critical aluminium level needed to form protective layers is estimated as 7–12 at-%, depending on the chromium content.[15] Nevertheless, the amounts of chromium and aluminium needed to produce protective oxides at low oxygen pressures can be different from those at high oxygen partial pressures. Current research articles also include the influence of HCl and H_2S on Fe–Cr–Al alloys in oxidising and reducing fuel derived environments.[15] Most of these experiments show that the presence of sulphur and chlorine are deleterious for the corrosion resistance of Fe–Cr–Al preventing the growth of alumina scales and causing the formation of less protective scales (a mixture of Fe, Cr and Al oxides). However, this topic needs to be further investigated to gain a better understanding of the behaviour of these materials and the mechanisms that govern them.[15]

One solution to protect heat exchanger materials and thereby improve their lives in a power plant would be the development of new coating compositions that can provide suitable protection by oxidation of chromium and aluminium to produce protective oxide layers at elevated temperatures. Such coatings would ensure longer component lives and could also allow higher steam operating temperatures in power plants fired on biomass or co-fired with a high biomass fuel fraction.[4,14]

In this paper eleven different coating compositions were applied onto sapphire discs using two targets (99·95 wt-%Cr and Fe–30 wt-%Al) using a magnetron sputtering technique. Later the samples were exposed in air and air–315 vpm HCl environments at 550°C for 150 h. After exposures all the specimens were carefully examined in an Environmental Scanning Electron Microscope (ESEM) and a Field Emission Gun SEM (SFEG) both combined with energy dispersive X-ray (EDX) spectroscopy, as well as by X-ray diffraction (XRD). The traditional mass change method has also been used to identify the oxidation/corrosion damage to the coatings.

Experimental methods

Materials

The coatings were deposited onto sapphire discs (10 mm diameter, 3 mm thick). Prior to deposition these were ultrasonically cleaned with water, then acetone and then IPA (isopropyl alcohol) before being placed in a specially designed sample holder (Fig. 1) to arrange them between two sputtering targets. Two groups of eleven coatings with different compositions were manufactured as a part of this study (as parallel lines of samples in the same period of coater operation).

A range of coating compositions was applied using the physical vapour deposition (PVD) method with a multi-target magnetron sputtering system. In this case two metal disc sources of (a) pure (99·95 wt-%) Cr and (b) Fe–30 wt-%Al were sputtered for 4 h and 35 min to obtain coatings with an average thicknesses of ~5 μm (maximum thickness of 9·35 μm (closer to the Cr target) and minimum thickness of 3·04 μm (closer to the Fe:Al target)). The thicknesses of coatings were investigated using a Veeco Dektak 3ST Surface Profiler (Santa Barbara, California). The groups of 11 samples were labelled as A–K, with the A samples placed directly below the chromium target and the K samples below the Fe:Al target.

High temperature oxidation in air and air with HCl

Before their exposure, the samples were weighed in a Sartorius CP225D balance and then placed in ceramic boats. Eleven samples (A–K) were exposed in a laboratory air environment in a horizontal furnace at 550°C. The samples were exposed in the furnace for 150 h (2 cycles were carried out: 50 h, then 100 h). After each exposure cycle, the samples were cooled down to room temperature and weighed.

For the air with HCl exposure, a further eleven samples were exposed. These samples were placed in an alumina-lined vertical furnace with controlled

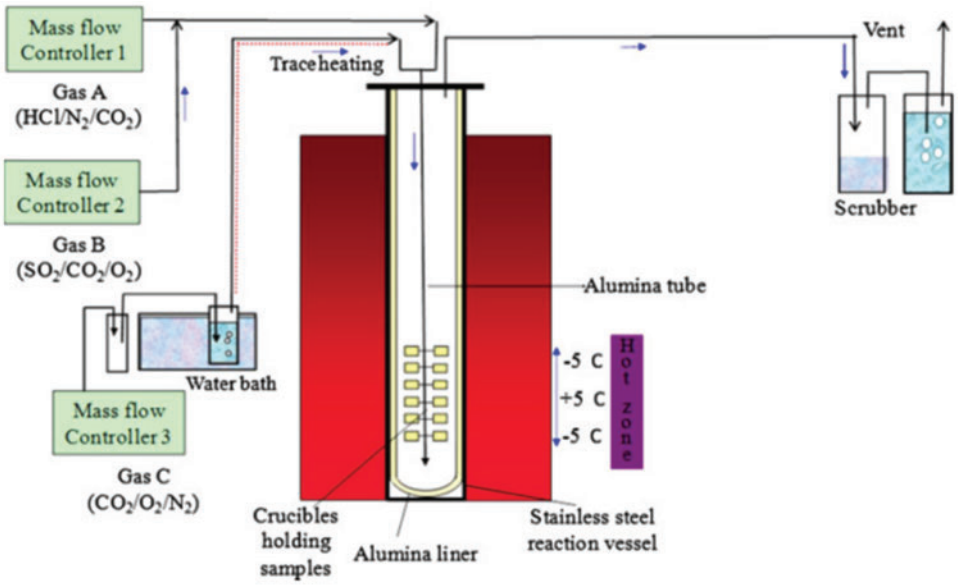

2 Schematic diagram of controlled atmosphere furnace setup for experiments in air with HCl[4]

atmosphere (Fig. 2) in air with 315 vppm HCl at 550°C (with a gas flowrate of 47 cc min^{-1}). This setup was used to simulate the gaseous part of the fireside corrosion conditions of superheaters/reheaters in biomass fired power plants. The furnace accommodates 24 samples at once in alumina crucibles in the hot zone (within ±5°C of the target temperature). To achieve the desired gas composition, air and HCl were pre-mixed and supplied to the furnace through the mass flow controllers. The pre-mixed gas entered the alumina reaction vessel from a central tube near its base (Fig. 2) before moving upwards to the exit at its top. The exhaust gas produced during the test passed through first an empty bottle to trap the condensate and next a bubbler (scrubber) containing NaOH solution, before venting to the atmosphere.[4] Contamination of samples by cross-evaporation was restricted by placing them in individual crucibles on a series of six levels separated by alumina plates.

Before the test these samples were weighed and put into individual alumina crucibles. Similar to air oxidation, the samples were exposed for 150 h in two cycles (50 and 100 h). After each exposure cycle, the samples were cooled down and weighed.

Surface analysis and coating characterisation

Before and after each test, the microstructures of the coatings and the morphology of the scales generated were characterised using an ESEM (Philips XL30, FEI) with EDX (Oxford Instruments, Aztec system) to determine the elemental composition of the oxidation/corrosion products. The EDX analysis was carried out using settings of 20 kV accelerating voltage, a spot size of 5 and at a 10 mm working distance. As expected for conventional EDX systems errors are typically ±0·1 at-% for concentrations <1 at-% and ±1 at-% for concentrations around 20 at-%.[18] X-ray diffraction (using a Siemens D5005) was carried out with a Cu K_α source at a wavelength of 0·1540 nm and a scan step of 0·02° to identify the phases formed on the samples' surfaces by the exposures.

Cross-sectional preparation and analysis

From the weight change data, the best performing samples in both the air and the air with HCl exposures were identified as samples D, E, F. These samples were mounted in a low shrinkage cold-setting resin with the addition of 50 vol.-% ballotini (to reduce further shrinkage). When the resin was set, the specimens were cross-sectioned using a precision cutting saw with a diamond blade and ground with a series of SiC papers before being polished first with 1 μm diamond paste and then using 0·05 μm colloidal silica. These sample cross-sections were prepared with non-aqueous lubricants to avoid dissolving any corrosion products. A high resolution SFEG (Philips XL30, FEI) was used to investigate the thicknesses of the scales and microstructures of the polished cross-sections. The samples were coated with a thin layer of Au and Pd before SFEG examination to make the samples conductive. The samples were investigated at magnifications of up to ×10 000 in the high resolution mode. EDX spectroscopy (operated at 20 kV with spot size 5) was used to identify the composition of the coatings and scales on the cross-sections.

Results

The as-deposited coatings were homogeneous in microstructure with only small variations in chemical compositions indicated by the EDX data; Figure 3 gives an example of the appearance of an unexposed coating surface. The compositions of the coatings exposed in both tests are given in Table 1 and illustrated in a Fe–Cr–Al ternary diagram (Fig. 4). For each sample, the measurements were performed in the sample's central region on an area of 150 × 120 μm. Similar regions were studied in the ESEM before and after the exposure for comparison purposes. The thickness of individual sample was found to vary by ~0·64 μm, indicating an even coating deposition.

Following their air, or air with HCl, exposures the surface compositions of the samples were measured with EDX again and these data are presented in Table 2. During their exposures in either of the two different gases, all the coatings had formed oxides. It should be noted that these EDX measurements were carried out looking down onto the top of the oxidised coatings and

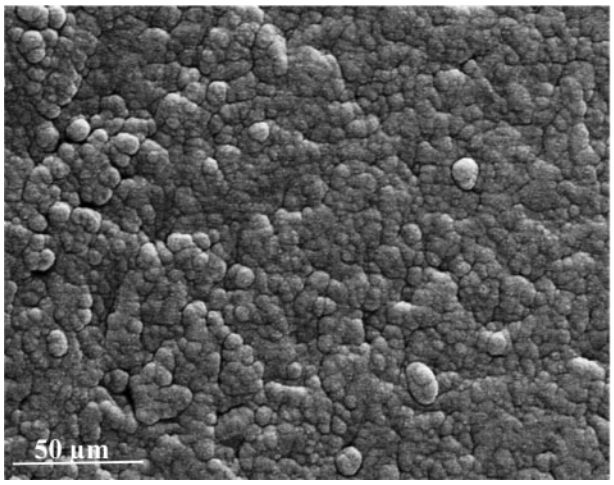

3 Surface morphology of coating before exposure (secondary electron image)

exposure were enriched in Cr or Al, depending on the initial coating compositions. For example, the Al/Fe ratio in the pre-exposure data (Table 1) for coating J to be exposed in air was 0·77, whereas after exposure it was 4·28. This effect could not be found in the EDX data from the exposure in air with HCl, with the pre-exposure Al/Fe ratio for coating J being 0·74 and the post-exposure ratio being 0·78 (i.e. approximately the same given the errors associated with EDX measurements); however, the thinner oxides found may have made this effect more difficult to detect.

The surface morphologies of the oxidised Fe–Cr–Al coatings are shown in Fig. 5. No significant difference was observed between the samples oxidised in air and those oxidised in air with HCl. The surfaces appeared to be more cracked for samples placed closer to the Fe–Al target (and so containing less chromium). On the surface of sample F exposed to air with HCl (identified as

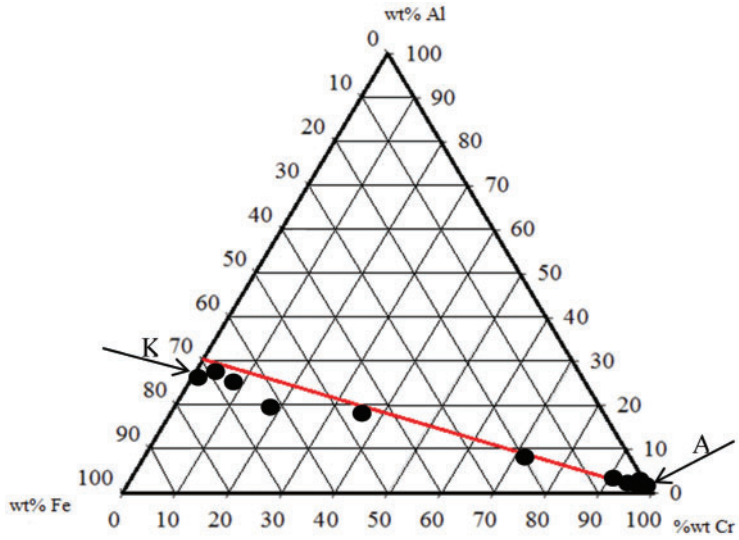

4 Ternary phase diagram of Fe–Cr–Al with coating composition for samples A–K (wt-%)

that the levels of oxygen measured (Table 2) indicate that the EDX analysis volumes penetrated through the oxide and into the coatings; hence these compositions include contributions from both the oxides formed and the underlying coatings. Lower levels of oxygen were measured for the samples exposed to air with HCl, indicating thinner oxide layers were present. The EDX data indicated that the oxidation products from the air sample F4), small pits can be observed but no spallation. EDX measurements indicate higher Al contents in some of those pitted areas (25 at-%) in comparison to the surrounding area (15 at-%). A slightly higher amount of Cl was detected close to the pits (0·2 at-%), whereas the surrounding areas registered 0·1 at-%Cl. Thus, this pitting damage might have been related to the presence of HCl in the atmosphere, but it should be noted that

Table 1 Composition of coatings before their furnace exposures (surface EDX data)

Sample	Composition of coatings exposed in air/at-%			Composition of coatings exposed in air with HCl/at-%		
	Cr	Fe	Al	Cr	Fe	Al
A	99·4	0·4	0·2	98·3	1·1	0·6
B	98·8	0·7	0·5	97·8	1·1	1·0
C	98·1	0·9	1·0	95·9	2·5	1·6
D	95·8	2·5	1·7	91·2	5·2	3·6
E	89·1	6·8	4·2	80·3	11·7	8·0
F	68·1	18·3	13·6	49·6	28·9	21·5
G	33·4	39·3	27·3	27·4	42·5	30·1
H	16·9	51·4	31·7	11·9	51·8	36·3
I	6·2	54·6	39·2	4·3	55·0	40·7
J	2·7	54·9	42·5	2·4	56·0	41·6
K	1·7	59·1	39·2	1·4	55·4	43·2

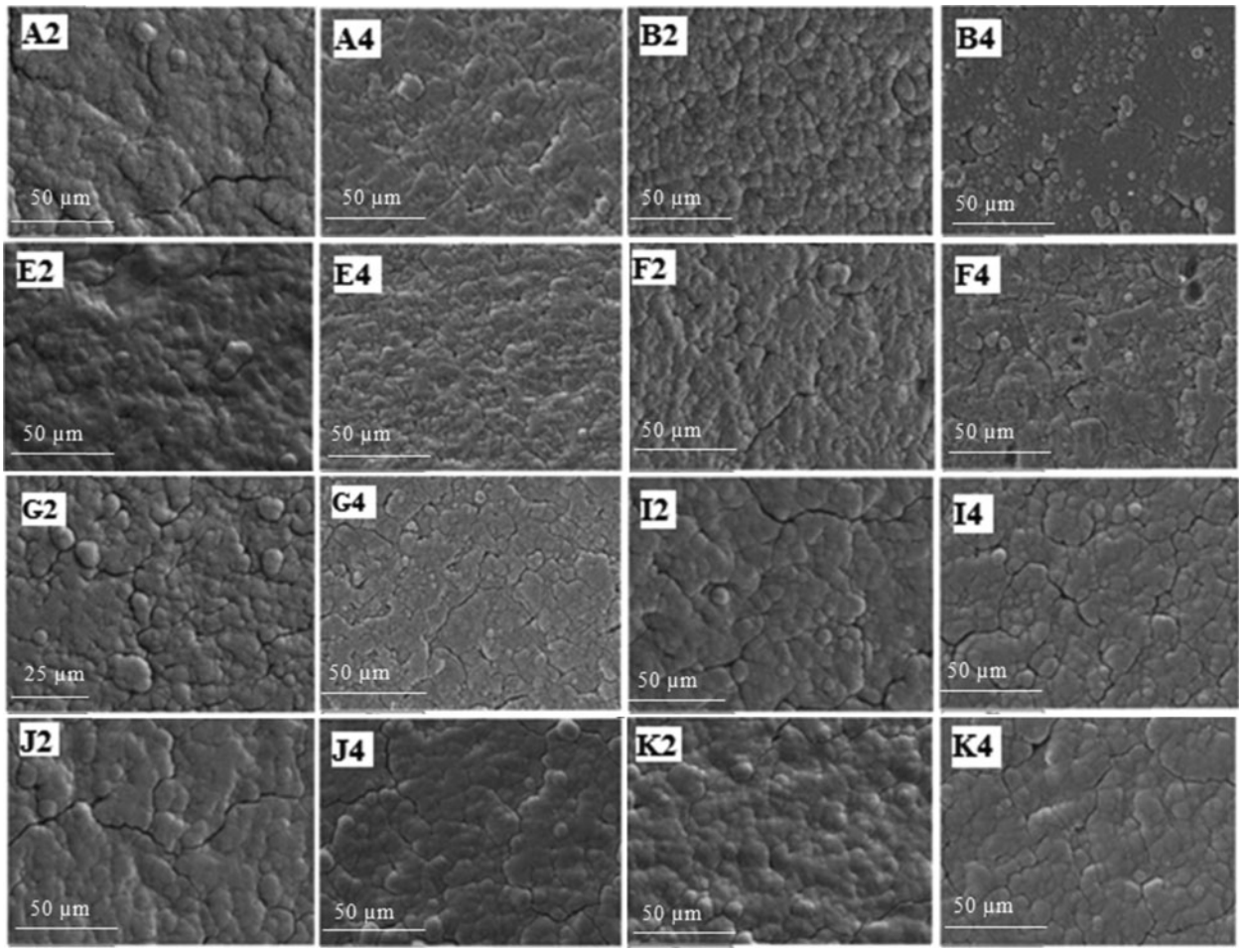

5 Surface morphologies of Fe–Cr–Al coatings after 150 h exposures in air and air with HCl atmospheres (secondary electron detector): samples A2–K2 were exposed in air and A4–K4 were exposed in air with HCl

these differences in Cl levels are at the limits of detection.

Two coatings (A and K) were investigated with XRD in order to compare phases formed before and after the tests (Fig. 6). For sample A, the three most characteristic peaks (44·5°, 64·5°, 81·7° 2θ) correspond to the α-Cr phase. In case of sample K, four peaks can be identified (30·9°, 44·2°, 64·1°, 81·1°) corresponding to the phase FeAl.

Twenty two XRD spectra (one for each sample) are shown in Figs. 7 and 8 after exposure in air and air with HCl respectively. These XRD results show that the X-ray beam penetrated the thin oxide layers on top the samples and detected phases (e.g. FeCr) from the bulk coating. From these XRD results, it can be seen that, for both atmospheres, the exposed coatings formed the same crystalline compounds (Table 5). Linked with the SEM observations, these results showed that several samples are covered with a thin layer of Cr_2O_3 (~1–2 μm) especially those created closer to the chromium target. On two samples (J and K) richer in Fe/Al, $FeAl_2O_4$ was detected, although the identification of this species was quite difficult due to the number of peaks and the differences in intensity. The most intense XRD peaks indicate the underlying coatings in each sample (as the X-rays had penetrated through the oxide layers). Depending on the coating composition they were either close to chromium (Cr), iron-chromium (FeCr) or iron–aluminium (FeAl). The intensity of the peak at 64·5° falls for samples D (air) and E (air and HCl), which could indicate a decreasing Cr phase content in the sample. Sample E (air) showed a very high peak at 81° which probably overlaps two intense peaks at the same position – from Cr and FeCr.

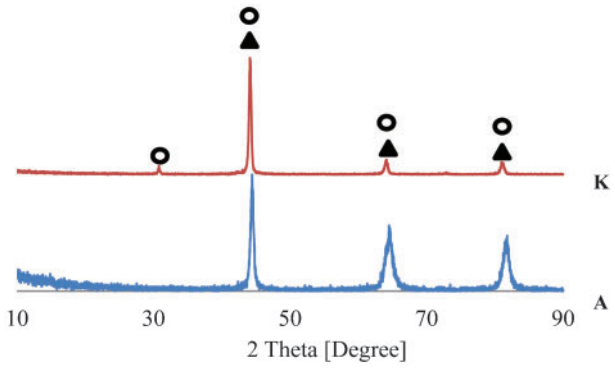

6 XRD spectra of sample A and sample K before exposure: symbols indicate: Cr (▲), AlFe (○)

Figures 9 and 10 show images from cross-sections through coatings D, E and F exposed to both atmospheres (at ×1 500 and ×10 000 magnifications respectively). Figure 9 shows where EDX analyses were carried out, with arrows indicating the 'top' and 'central' areas used to generate the data given in Tables 3 and 4 respectively. The oxygen contents in all these analyses indicate that the EDX analysis volumes have included

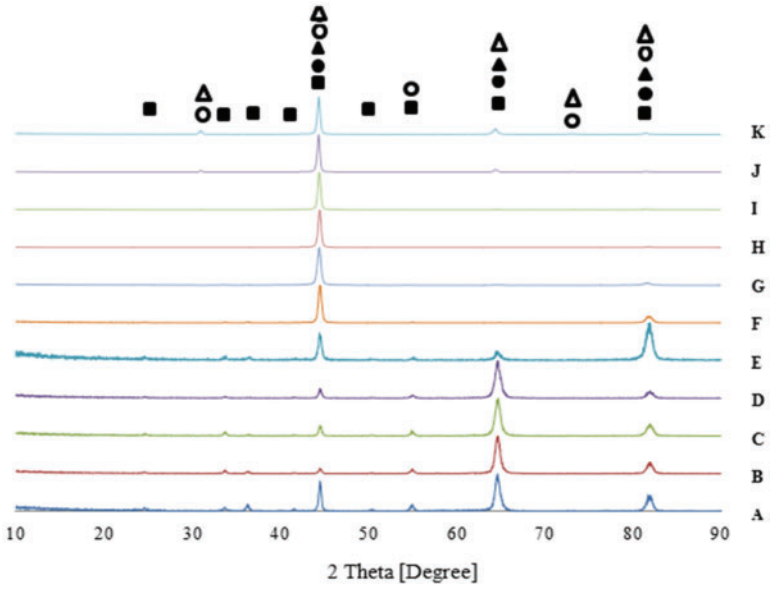

7 XRD spectra of Fe–Cr–Al coatings oxidised in air at 550°C for 150 h: symbols indicate: Cr_2O_3 (■), FeCr (●), Cr (▲), AlFe (○), $FeAl_2O_4$ (Δ)

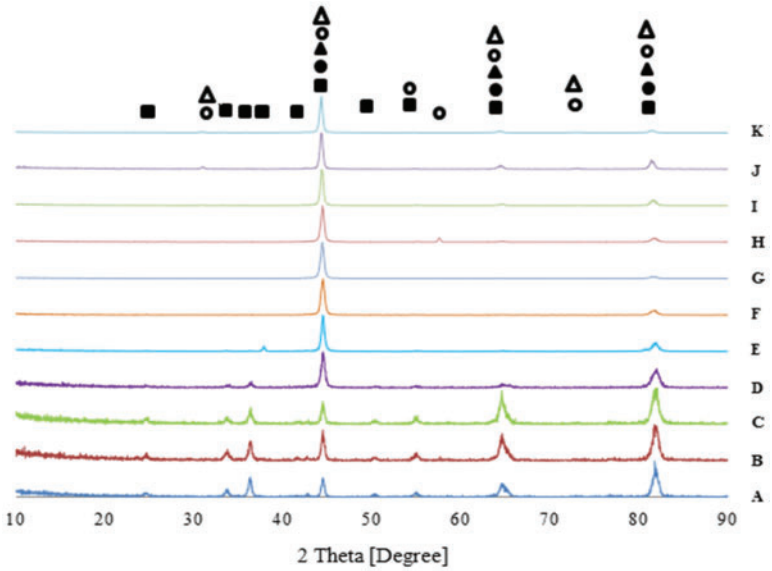

8 XRD spectra of Fe–Cr–Al coatings oxidised in air with HCl at 550°C for 150 h: symbols indicate: Cr_2O_3 (■), FeCr (●), Cr (▲), AlFe (○), $FeAl_2O_4$ (Δ)

Table 2 Coating compositions after 150 h of exposure in air and air with HCl environments (surface EDX data)

	Elemental composition after oxidation in air/at-%				Elemental composition after oxidation in air with HCl/at-%				
Sample	Cr	Fe	Al	O	Cr	Fe	Al	O	Cl
A	48·2	0·1	0·1	51·6	62·5	0·6	0·5	36·4	0·1
B	66·1	0·3	0·5	33·1	63·7	1·1	0·8	34·3	0·1
C	64·9	0·7	0·6	33·8	65·9	1·9	1·2	30·9	0·1
D	55·1	1·3	1·8	41·9	62·7	4·0	2·7	30·5	0·1
E	59·1	3·7	3·6	33·6	59·4	8·6	5·9	25·9	0·1
F	30·4	5·8	13·1	50·7	39·5	18·7	14·9	26·8	0·1
G	8·1	3·9	23·9	64·2	21·9	32·7	23·4	21·7	0·2
H	4·6	7·7	34·6	53·2	9·1	38·8	29·3	22·6	0·2
I	1·5	7·9	35·5	55·1	3·9	39·3	31·3	25·3	0·2
J	0·7	9·4	40·2	49·7	2·1	45·4	35·6	16·9	0·0
K	0·4	5·5	39·5	54·7	1·2	44·4	33·5	20·8	0·1

parts of both the coatings and the oxide scales generated. The data from the coatings exposed in the air with HCl atmosphere show Cl contents of up to 0·5 at-%. The higher magnification ($\times 10\,000$) images given in Fig. 10 show that all the coatings have thin surface oxides and are dense with columnar microstructures (and have experienced varying degrees of damage during sample preparation).

The final weight change results are given in Table 5, together with the phases detected by XRD after 150 h in the two different atmospheres. In the air environment six samples indicated mass loss (0·6–0·9 mg cm^{-2}) and the rest showed mass gain (0·1–0·3 mg cm^{-2}). Samples D, E, F showed similar, low mass change (~0·1 mg cm^{-2}) and so may be considered the most stable compositions (68–96 at-%Cr, 3–18 at-%Fe, 2–14 at-%Al). In the air with HCl atmosphere, three samples showed mass losses (of 0·3–0·9 mg cm^{-2}) but the other eight specimens resulted in mass gains (of 0·1–0·7 mg cm^{-2}). No spalled scale was observed in the sample crucibles. Samples E and F (with coating compositions of 50–80 at-%Cr, 12–29 at-%Fe, 8–22 at-%Al) showed the lowest mass change (0·1–0·2 mg/cm^2) and these were two of the sample compositions that were the most stable in the air exposure too. Thus, the composition range 50–96 at-%Cr, 3–29 at-%Fe, 2–22 at-%Al (from samples D, E and F) provides good protection at high temperatures; however, further investigations must be carried out to confirm their good performance and narrow the composition range.

Discussion

It was expected that the addition of HCl to air could have had a significant effect on the coatings and enhanced their oxidation. However, for all the specimens investigated in the air with HCl environment, only low levels of chlorine were detected using EDX on the sample surfaces (0·1–0·2 at-%). As these analyses had penetrated through the oxide layer and into the coatings, the location of this chlorine within/around the oxide layer could not be identified. However, EDX analyses from cross-sectioned samples showed slightly higher levels of chlorine (between 0·4–0·5 at-%) in areas of coatings close to (and partially including) the oxide layer. Given the EDX analysis volumes, this could suggest that the chlorine was higher at the metal/oxide interface, as anticipated from previous work.[11] It is possible that some metal chlorides had formed and evaporated into the atmosphere. Chloride induced corrosion problems have been widely investigated and it is known from the literature that Cl_2 is more aggressive than HCl and increases the corrosion rate. In oxidising atmospheres Cl_2 is formed from HCl gas according to the reaction below[19]

$$4HCl(g) + O_2(g) = 2Cl_2(g) + 2H_2O \quad (1)$$

The stability of the metal chlorides and oxides that are formed in oxidising atmospheres containing chlorine depends on the partial pressure of oxygen and chlorine. Chlorides are stable at the metal/oxide interface because

Table 3 Compositions of cross-sectioned samples measured close to top of coatings (as indicated by arrows in Fig. 9)

	Elemental composition after oxidation in air/at-%				Elemental composition after oxidation in air with HCl/at-%				
Sample	Cr	Fe	Al	O	Cr	Fe	Al	O	Cl
D	77·9	3·0	2·0	17·0	40·2	3·0	1·6	22·9	0·4
E	72·2	6·7	3·9	15·9	61·8	9·9	6·7	21·1	0·5
F	40·1	9·8	7·2	13·1	53·2	25·3	15·0	6·0	0·5

Table 4 Compositions of cross-sectioned samples measured in middle of coatings

	Elemental composition after oxidation in air/at-%				Elemental composition after oxidation in air with HCl/at-%				
Sample	Cr	Fe	Al	O	Cr	Fe	Al	O	Cl
D	89·9	2·0	1·8	6·3	75·3	5·8	3·5	15·1	0·3
E	79·6	6·1	4·3	10·0	70·1	8·9	6·6	13·9	0·5
F	61·9	12·9	8·8	15·0	52·2	25·4	15·7	6·4	0·4

Table 5 Mass change and possible phases after exposures

	After oxidation in air		After oxidation in air with HCl	
Sample	Final mass change/mg cm^{-2}	Phases from XRD	Final mass change/mg cm^{-2}	Phases from XRD
A	0·25	Cr_2O_3, Cr	0·48	Cr_2O_3, Cr, FeCr
B	−0·82	Cr_2O_3, Cr	0·39	Cr_2O_3, Cr, FeCr
C	−0·77	Cr_2O_3, Cr, FeCr	−0·27	Cr_2O_3, FeCr
D	0·10	Cr_2O_3, Cr, FeCr	0·32	Cr_2O_3, Cr, FeCr
E	0·10	Cr_2O_3, Cr, FeCr	0·13	Cr_2O_3, FeCr
F	0·11	AlFe, Cr, FeCr	0·23	AlFe
G	−0·88	Cr, AlFe	0·65	AlFe
H	−0·68	Cr, AlFe	−0·88	AlFe
I	0·08	Cr, AlFe	0·24	AlFe
J	−0·86	AlFe, $FeAl_2O_4$	0·28	AlFe, $FeAl_2O_4$
K	−0·64	AlFe, $FeAl_2O_4$	−0·80	AlFe, $FeAl_2O_4$

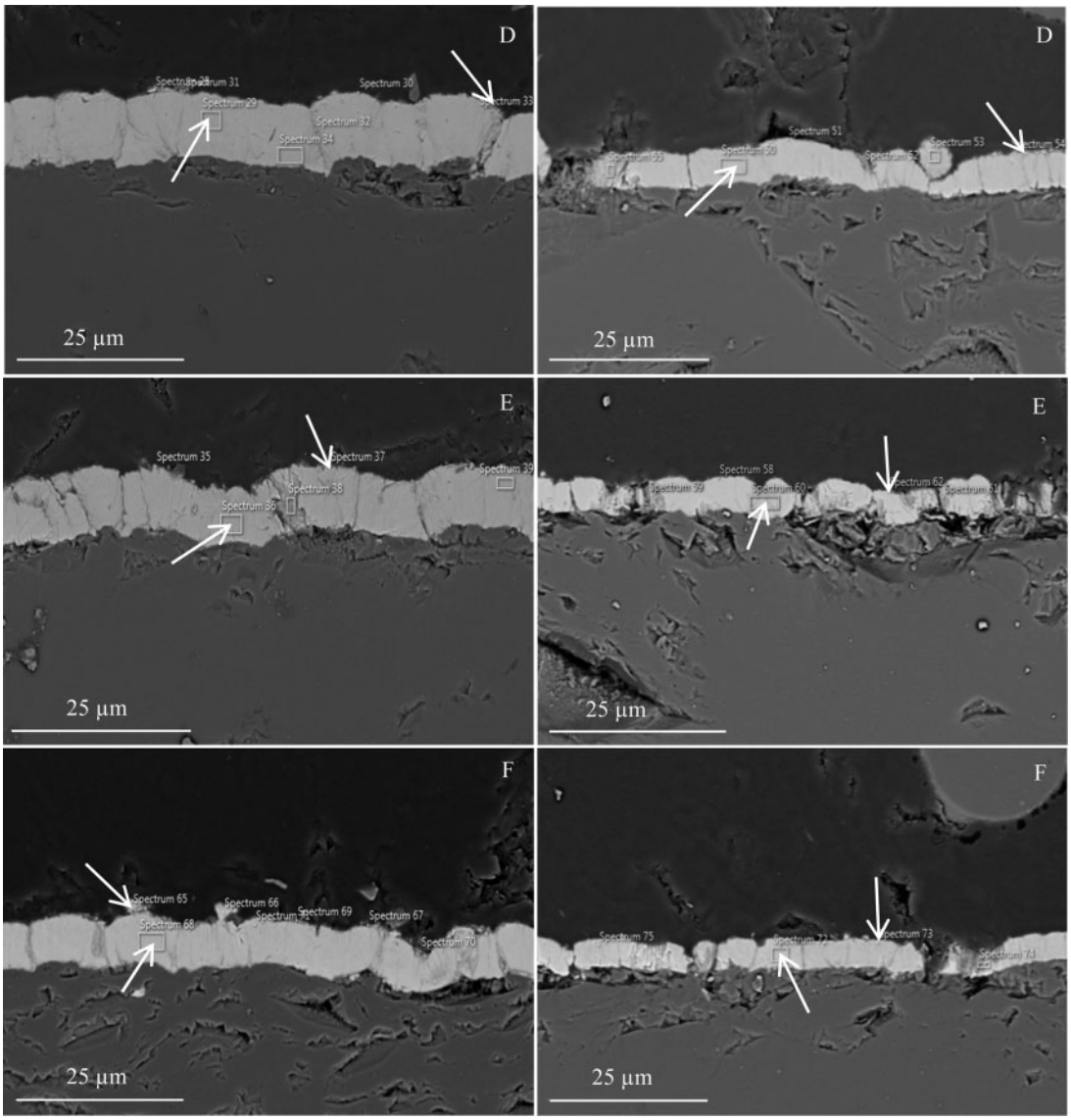

9 Cross-sections through coatings D, E and F after exposure in air (left column) and air with HCl (right column) – SFEG, BSE detector: EDX results from areas indicated by arrows are shown in Tables 3 and 4

the oxygen partial pressure is low. Considering different coating compositions a few different volatile solid and gaseous metal chlorides could form (equation (2))[19]

$$2M(s)+Cl_2(g)=2MCl_2(s,g) \quad (2)$$

Chlorides may evaporate and diffuse to the gas/scale interface and on reaching the higher oxygen partial pressure release chlorine. This mechanism is called 'active oxidation' (equation (3))[19]

$$2MCl_2(g)+3/2O_2(g)=M_2O_3(s)+2Cl_2(g) \quad (3)$$

There was no sign of iron oxide Fe_2O_3 in the samples. It is known from the literature[19,20] that the partial pressure of oxygen needed to convert the iron chloride into oxide is higher than the partial pressure of oxygen required to transform chromium chloride into oxide. Also, the Gibbs free energy of the formation of chromium chlorides is more negative than that of formation of iron chlorides (see equations (4)–(6)).[19,20] This means that chromium chloride will be preferably formed first from the base metal below the oxide layer. Following this, chromium oxide will be formed closer to the metal surface than iron oxide[19]

$$Fe+Cl_2=FeCl_2 \quad (4)$$

ΔG (at 550°C)$=-238$ kJ mol^{-1}; partial pressure of $FeCl_2$ (at 550°C)$=2{\cdot}1\times10^{-4}$ bar

$$Cr+Cl_2=CrCl_2 \quad (5)$$

ΔG (at 550°C)$=-292$ kJ mol^{-1}; partial pressure of $CrCl_2$ (at 550°C)$=2{\cdot}0\times10^{-7}$ bar

$$2Al+3Cl_2=2AlCl_3 \quad (6)$$

ΔG (at 550°C)$=\sim(-541)$ kJ mol^{-1}; partial pressure of $AlCl_3$ (at 550°C)$=\sim1$ bar

Chlorides that evaporate and are not converted to oxides within the scale, but diffuse into the atmosphere cause a mass loss from the sample.[19] Whilst thinner oxides are observed on the samples exposed in the air with HCl atmosphere, the mass change data produced only showed mass losses for three samples (C4: 0·3 mg cm^{-2}, H4: 0·9 mg cm^{-2}, K4: 0·8 mg cm^{-2}). Thus, further data is required to prove whether metal chloride species were evaporating into the flowing gas atmosphere.

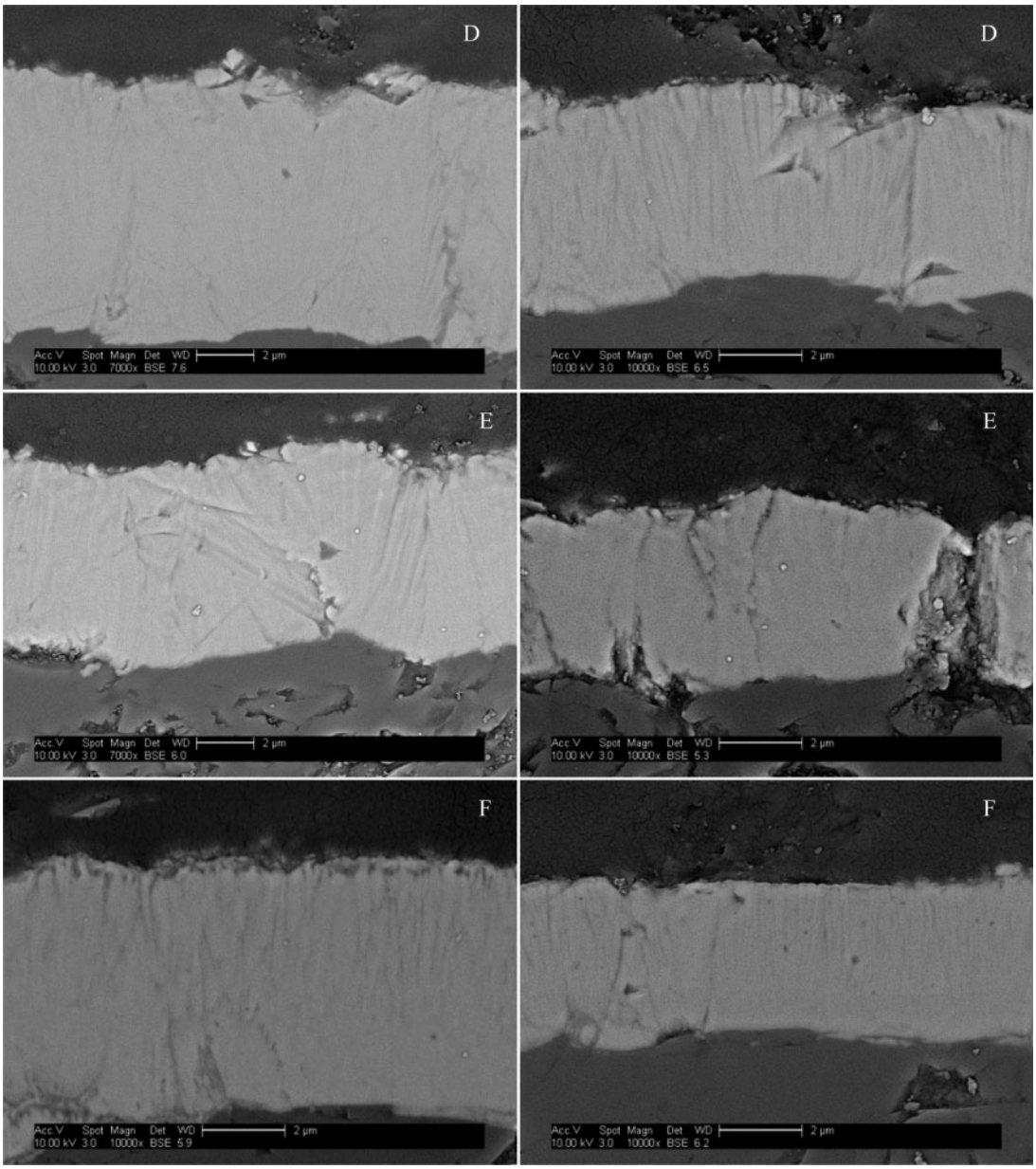

10 Higher magnification images of cross-sectioned samples D, E and F after air (left column) and air with HCl (right column) exposures (SFEG, BSE images)

Conclusions

The magnetron sputtering technique was successfully used to produce a range of Fe–Cr–Al coatings on the sapphire discs by co-sputtering from two sources (Cr and Fe–30Al). The XRD, SEM/EDX and traditional mass change method were used to characterise the samples after the exposure in two oxidising atmospheres (air with and without 315 ppm HCl) at 550°C.

Depending on the coating's composition, either Cr_2O_3 or $FeAl_2O_4$ was observed. The oxides formed were very thin, which resulted in getting strong diffraction peaks from the underlying coatings. Regardless of the atmosphere the same XRD peaks were detected for both exposures indicating the formation of the same crystalline phases.

The weight change data showed the smallest values for samples D, E and F with a composition range: 50–96 at-%Cr, 3–29 at-%Fe, 2–22 at-%Al. Those three compositions may be considered the most stable in these conditions and will be further investigated using simulated combustion gases and chloride containing deposits. The presence of HCl in the gaseous environment did not appear to cause any significant changes in oxidation mechanisms; a very small amount of chlorine was detected on the sample surfaces but there was no sign of enhanced oxidation. Further investigations are required to determine the possible mechanisms that control the role of HCl.

The microstructures of the coatings were cracked, which may indicate residual stresses that were relieved within them. This cracking increased with increasing Fe–Al content in the coatings.

Acknowledgements

This work is part of a PhD project on the development of novel coatings to resist fireside corrosion in

biomass-fired power plants funded by the Biomass and Fossil Fuels Research Alliance (BF2RA) and in cooperation with E.ON New Build & Technology Ltd.

References

1. T. Hussain, A. U. Syed and N. J. Simms: 'Fireside corrosion of superheater materials in coal/biomass co-fired advanced power plants', *Oxid. Met.*, Mar. 2013, **80**, (5–6), 529–540.
2. J. Pettersson, N. Folkeson, L. G. Johansson and J. E. Svensson: 'The effects of KCl, K_2SO_4 and K_2CO_3 on the high temperature corrosion of a 304-type austenitic stainless steel', *Oxid. Met.*, Mar. 2011, **76**, (1–2), 93–109.
3. S. Paul and M. D. F. Harvey: 'Corrosion testing of Ni alloy HVOF coatings in high temperature environments for biomass applications', *J. Therm. Spray Technol.*, Sep. 2012, **22**, (2–3), 316–327.
4. T. Hussain, T. Dudziak, N. J. Simms and J. R. Nicholls: 'Fireside corrosion behavior of HVOF and plasma-sprayed coatings in advanced coal/biomass Co-fired power plants', *J. Therm. Spray Technol.*, Jan. 2013, **22**, (5), 797–807.
5. N. Folkeson, T. Jonsson, M. Halvarsson, L. G. Johansson and J. E. Svensson: 'The influence of small amounts of KCl(s) on the high temperature corrosion of a Fe-2·25Cr-1Mo steel at 400 and 500°C', *Mater. Corros.*, Jul. 2011, **62**, (7), 606–615.
6. B.-J. Skrifvars, M. Westén-Karlsson, M. Hupa and K. Salmenoja: 'Corrosion of super-heater steel materials under alkali salt deposits. Part 2: SEM analyses of different steel materials', *Corros. Sci.*, Mar. 2010, **52**, (3), 1011–1019.
7. C. Pettersson, L. G. Johansson and J. E. Svensson: 'The influence of small amounts of KCl(s) on the initial stages of the corrosion of alloy Sanicro 28 at 600°C', *Oxid. Met.*, Aug. 2008, **70**, (5–6), 241–256.
8. H. P. Nielsen, F. J. Frandsen, K. Dam-Johansen and L. L. Baxter: 'The implications of chlorine-associated corrosion on the operation of biomass-fired boilers', *Prog. Energy Combust. Sci.*, Jun. 2000, **26**, (3), 283–298.
9. J. Lehmusto, B.-J. Skrifvars, P. Yrjas and M. Hupa: 'High temperature oxidation of metallic chromium exposed to eight different metal chlorides', *Corros. Sci.*, Oct. 2011, **53**, (10), 3315–3323.
10. T. Jonsson, J. Froitzheim, J. Pettersson, J.-E. Svensson, L.-G. Johansson and M. Halvarsson: 'The influence of KCl on the corrosion of an austenitic stainless steel (304L) in oxidizing humid conditions at 600°C: a microstructural study', *Oxid. Met.*, May 2009, **72**, (3–4), 213–239.
11. P. Viklund and R. Pettersson: 'HCl-induced high temperature corrosion of stainless steels in thermal cycling conditions and the effect of preoxidation', *Oxid. Met.*, Dec. 2010, **76**, (1–2), 111–126.
12. K. Messaoudi, A. Huntz and B. Lesage: 'Diffusion and growth mechanism of Al_2O_3 scales on ferritic Fe-Cr-Al alloys', *Mater. Sci. Eng. A*, Jun. 1998, **247**, (1–2), 248–262.
13. H. Josefsson, F. Liu, J.-E. Svensson, M. Halvarsson and L.-G. Johansson: 'Oxidation of FeCrAl alloys at 500–900°C in dry O_2', *Mater. Corros.*, Nov. 2005, **56**, (11), 801–805.
14. M. A. Uusitalo and T. A. Mantyla: 'High temperature corrosion of coatings and boiler steels in reducing chlorine-containing atmosphere', 2002, **161**, 275–285.
15. W. M. Lu, T. J. Pan and Y. Niu: 'Accelerated corrosion of Fe–xCr–10Al alloys containing 0–20 at.% Cr induced by sulfur and chlorine in a reducing atmosphere at 600°C', *Oxid. Met.*, Nov. 2007, **69**, (1–2), 63–76.
16. J. Engkvist, U. Bexell, M. Grehk and M. Olsson: 'High temperature oxidation of FeCrAl-alloys – 'influence of Al-concentration on oxide layer characteristics', *Mater. Corros.*, Nov. 2009, **60**, (11), 876–881.
17. L. Mare: 'Oxidation behavior of ODS Fe–Cr–Al alloys: aluminum depletion and lifetime', Aug. 2003, **60**, 1–28.
18. R. H. Geiss: 'Energy-dispersive X-ray spectroscopy, EDS', in 'Encyclopedia of Materials Characterization: surfaces, interfaces, thin films', (ed. C. R. Brundle *et al.*), 120–135; 1992, Greenwich, Manning Publications Co.
19. D. E. Von Legierungselementen: 'The influence of alloying elements on the chlorine-induced high temperature corrosion of Fe-Cr alloys in oxidizing atmospheres', 1999, **578**, pp. 561–578.
20. M. Uusitalo, P. M. Vuoristo and T. Mäntylä: 'High temperature corrosion of coatings and boiler steels below chlorine-containing salt deposits', *Corros. Sci.*, Jun. 2004, **46**, (6), 1311–1331.
21. M. Seraffon: 'Performances of air plasma sprayed thermal barrier coatings for industrial gas turbines', PhD thesis, Cranfield University, UK, 2012.